



HAL
open science

Phonon transmission at Si/Ge and polytypic Ge interfaces using full-band mismatch based models

Jérôme Larroque, Philippe Dollfus, Jérôme Saint-Martin

► **To cite this version:**

Jérôme Larroque, Philippe Dollfus, Jérôme Saint-Martin. Phonon transmission at Si/Ge and polytypic Ge interfaces using full-band mismatch based models. *Journal of Applied Physics*, 2018, 123 (2), 10.1063/1.5007034 . hal-01906686

HAL Id: hal-01906686

<https://hal.science/hal-01906686>

Submitted on 27 Oct 2018

HAL is a multi-disciplinary open access archive for the deposit and dissemination of scientific research documents, whether they are published or not. The documents may come from teaching and research institutions in France or abroad, or from public or private research centers.

L'archive ouverte pluridisciplinaire **HAL**, est destinée au dépôt et à la diffusion de documents scientifiques de niveau recherche, publiés ou non, émanant des établissements d'enseignement et de recherche français ou étrangers, des laboratoires publics ou privés.

Phonon transmission at Si/Ge and polytypic Ge interfaces using Full-Band mismatch based models

J. Larroque, P. Dollfus and J. Saint-Martin

Center of Nanoscience and Nanotechnology, CNRS UMR 9001, Univ. Paris-Sud, Université Paris-Saclay, 91405 Orsay, France

Abstract: This paper presents theoretical investigations on the interfacial thermal conductance (Kapitza conductance) in both monotype Si/Ge (cubic 3C) and polytype (cubic 3C / hexagonal 2H) Ge interfaces by using Full Band extensions of Diffusive (DMM) and Acoustic (AMM) Mismatch Models. In that aims, phonon dispersions in the Full 3D Brillouin Zone have been computed via an atomistic adiabatic bond charge model. The effects of crystal orientation are investigated and the main phonon modes involved in heat transfer are highlighted. According to our calculations, polytype interfaces without any mass mismatch but with a crystallographic phase mismatch exhibit a thermal conductance very close to that of Si/Ge interfaces with a mass mismatch but without any phase mismatch. Besides, the orientations of Ge polytype interface that have been observed experimentally in nanowires, i.e. along $[115]/[50\bar{5}1]$, exhibit the lowest interfacial conductance and thus may offer new opportunities for nanoscale thermoelectric applications.

I. INTRODUCTION

The heat transfer at the nanoscale is currently widely investigated both theoretically and experimentally [1]. Indeed, at this scale of the order of the phonon mean free path the macroscopic Fourier heat law assuming local thermal equilibrium tends to reach its limit of validity [2] [3]. In particular, the understanding of thermal transport across interfaces, that gives rise to a thermal resistance, also called Kapitza resistance [4][5], is a major issue. This is especially true given that recent developments in nanotechnologies, e.g. heteroepitaxy [6] or atomic bonding [7], make possible the fabrication of new classes of interfaces. In particular, interfaces between semiconducting materials of the column IV of the periodic table such as Si and Ge and/or III-V compounds open the way of performance enhancement in optoelectronics [8], thermoelectrics [9] and also electronics. For instance, tunnel Field Effect Transistors based on Si/Ge [10] or Si/InAs [11] interfaces are expected to improve the off-behavior of transistors.

Among the novel nanostructures promising for thermal engineering, polytype nanowires that can be fabricated in both Silicon [12] and Germanium [13] are appealing as they are compatible with mature technology developed for decades in microelectronic industry. Indeed, in these structures, nano-clusters crystallized in the 2H phase, a phase that cannot be stabilized in a bulk form under normal conditions, can be embedded in a standard 3C phase background. A kind of superlattice is formed in which many polytype interfaces are distributed quasi-periodically along the wire at a scale comparable to or smaller than the mean free path of phonons. This specific type of structuring should affect the internal heat transport.

In order to model the Kapitza resistance [9] [10], advanced atomistic Ab Initio [14] and Molecular Dynamics methods [15][16][17] have been used. However, these advanced approaches require a large amount of computational time and resources. Although MD simulation can currently manage up to tens of thousands atoms [18], their use is restricted in terms of temperature range that should be higher than the Debye temperature. In this work, we opted to use semi-analytical derivations of the heat (also called thermal) flux carried by phonons and conductance across interfaces, which allows us to easily manage complex interface orientations while capturing the anisotropic effects of phonon dispersion. Phonon transmissions were calculated by using the common Diffusive Mismatch Model (DMM) [5] and Acoustic Mismatch Model (AMM) [19]. Postulates of AMM and DMM correspond to two opposite ideal cases. A perfect interface (without scattering center) conserving the wave coherence is considered in AMM while DMM deals with a fully diffusive (rough and/or with many defects) interface breaking the wave coherence. The main originality of our approach is to take into account the actual Full Band (FB) phonon dispersion, i.e. the phonon dispersions considered in this paper have been computed in the entire (3D) Brillouin zone. Contrary to previous approaches assuming isotropic phonon dispersion [20], our FB approach enables the computation of the phonon transmission along different crystalline orientations.

In this work, the adiabatic bond charge model (ABCM) [21] was used to compute the phonon FB dispersion for each bulk material involved in the considered interface as presented in Ref. [22]. ABCM is a semi-empirical atomistic approach that is faster and easier to compute than ab-initio methods. Because of its efficiency, the ABCM has been used to calculate phonon dispersions in several materials [23] and in various silicon nanostructures such as nanocrystals [24]. In the present work, using these ABCM dispersions, the phonon transmission at an interface was derived via a Full Band extension of DMM and AMM. The FB extension for the DMM has been previously derived by Reddy et al.[25]. Here, we present our original derivation of the FB extension for the AMM.

The paper is organized as follows. Semi-analytical Full-Band models of the transmission are presented in Section 2. Interfacial thermal conductance at monotype Si/Ge and Ge polytype interfaces are studied in Sections 3 and 4, respectively. Several crystalline orientations and the corresponding spectral conductance are investigated.

II. INTERFACIAL THERMAL CONDUCTANCE MODELING

To compute the phonon transmission at an interface between two materials or two phases of the same material, as schematized in FIG. 1, we have chosen to use simple but versatile semi-analytical approaches based on AMM and DMM extended to the full-band description of phonon dispersions. The full-band dispersion of bulk materials involved in the interface are computed

within the semi-empirical ABCM approach. The FB dispersions for Si and Ge in both cubic (3C) and (2H) hexagonal phases are reported in Ref. [22]. It should be noted that the BZ of the studied materials is typically sampled in $64 \times 64 \times 64$ cubes.

In this section, we successively describe the Full-Band extension of AMM, Pseudo-AMM (PAMM) that is a model derived from AMM and finally DMM.

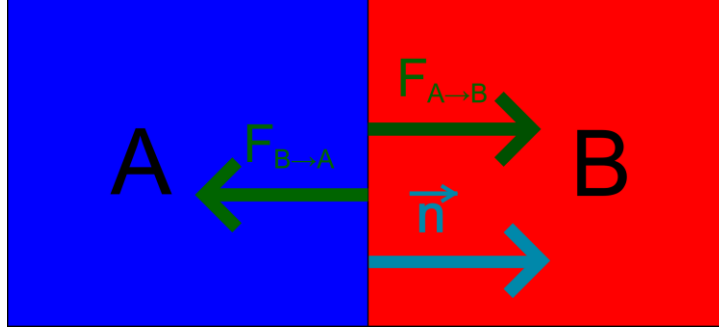


FIG. 1: Schema of thermal flux at an interface between materials A and B.

II.1. Full-Band AMM

The basic assumption underlying the Acoustic Mismatch Model [19] is to consider an ideal interface without any defect i.e. without any scattering center. It implies that the thermal wave coherence is conserved and the phonon transmission only depends on the incident wave vector. Moreover, both the phonon energy and flux across the interface must be conserved too. In the standard version of AMM introduced by Little [19], the phonon mode (i.e. phonon frequency and polarization) is also conserved during the interface crossing. It should be mentioned that this approach indirectly ensures the principle of detailed balance i.e. the thermal fluxes in both directions are equal at equilibrium ($F_{A \rightarrow B} = F_{B \rightarrow A}$, see FIG. 1).

In this formalism, for each mode m , three kinds of wave functions are considered at the interface: the incident waves $\Psi_i(\vec{r})$, the reflected waves $\Psi_r(\vec{r})$ and the transmitted waves $\Psi_t(\vec{r})$. Within a Full Band description, each of them consists in a linear combination of several plane waves in the form of

$$\Psi_{i(r/t)}(\vec{r}) = \sum_{j=1}^{N_{i(r/t)}} A_{i(r/t),j} \times \exp(i \vec{q}_{i(r/t),j} \cdot \vec{r}) \quad (1)$$

Where the indexes i , r and t stand for incident, reflected and transmitted waves, respectively. $A_{i(r/t),j}$ and $\vec{q}_{i(r/t),j}$ are the amplitude and wave vector, respectively, of the j^{th} incident (/reflected/transmitted) wave. All the $\vec{q}_{i(r/t),j}$ involved in the

summation present in Eq. 1 are related via phonon dispersion to the same angular frequency $\omega = \omega(\vec{q}_{i(r/t),j})$ to ensure energy conservation. The wave vectors must have also the same parallel component of their wave vector \vec{q}_{\parallel} (component perpendicular to vector \vec{n} schematized in FIG. 1) to fulfill the AMM requirements (demonstrated just below). Thus, let's define the number N_i (N_r and N_t) as the number of incident (reflected and transmitted, respectively) plane waves meeting the two above criteria. It leads us to consider a set of waves $\Psi_i(\vec{r})$, $\Psi_r(\vec{r})$ and $\Psi_t(\vec{r})$, depending only on both parameters ω and \vec{q}_{\parallel} .

The perpendicular flux operator \hat{J}_{\perp} (flux along vector \vec{n} in FIG. 1) and the transmission coefficient $T_{A \rightarrow B}$ from material A to material B are defined as:

$$J_{\perp} \Psi_{i(r/t)} = \sum_{j=1}^{N_{i(r/t)}} |A_{i(r/t),j}|^2 \times v_{g,i(r/t),j}^{\perp}$$

$$T_{A \rightarrow B} = \frac{\hat{J}_{\perp} \Psi_t}{\hat{J}_{\perp} \Psi_i}$$

Where $v_{g,i(r/t),j}^{\perp}$ is the perpendicular group velocity of the j^{th} incident(/reflected/transmitted) plane.

To ensure the conservation of the phonon flux probability across the interface, i.e. $\hat{J}_{\perp} \Psi_i - \hat{J}_{\perp} \Psi_r = \hat{J}_{\perp} \Psi_t$, and the continuity of the wave function at the interface S_{int} , i.e. $\Psi_i(\vec{r}) + \Psi_r(\vec{r}) = \Psi_t(\vec{r})$ for $\vec{r} \in S_{\text{int}}$, the parallel component of the wave vector must be conserved, leading to $\vec{q}'' = \vec{q}_{i,j}'' = \vec{q}_{r,j}'' = \vec{q}_{t,j}''$ (as already mentioned in comments on Eq.1).

Besides, if all plane waves are assumed to have the same amplitude, i.e. $A_{i(r/t),j} = A_{i(r/t)}$ for any j in Eq. 1, and defining

$$\alpha = \frac{|A_r|}{|A_i|}, \quad \beta = \frac{|A_t|}{|A_i|} \quad \text{and} \quad v_{i/r/t} = \frac{1}{N_{i/r/t}^2} \sum_{j=1}^{N_{i/r/t}} v_{g,i/r/t,j}^{\perp}, \quad \text{we arrive at the following set of equations:}$$

$$\begin{cases} N_i^2 \times v_i - N_r^2 \times v_r \times \alpha^2 = N_t^2 \times v_t \times \beta^2 \\ N_i + N_r \times \alpha = N_t \times \beta \\ T_{A \rightarrow B}(\vec{q}_{\parallel}, \omega) = \frac{v_t}{v_i} \times \frac{N_t^2}{N_i^2} \times \beta^2 \end{cases}$$

Finally, the transmission coefficient for a mode m can be analytically derived as:

$$T_{A \rightarrow B}(\vec{q}_{\parallel}, \omega, m) = \frac{v_t}{v_i} \left(\frac{v_r + \sqrt{v_r v_i + v_i v_t - v_t v_r}}{(v_t + v_r)} \right)^2 \quad (2)$$

In our FB-AMM algorithm, the transmission is computed for each angular frequency ω , for each component of wave vector parallel to the interface \vec{q}_{\parallel} , and for each mode. For each material, all possible incident, reflected and transmitted waves that have a relevant parallel wave vector with an angular frequency ω (energy conservation) in the Full 3D Brillouin Zone are listed to get the related transmission coefficient.

Besides, within a Landauer formalism, the expression of thermal flux $F_{A \rightarrow B}(T)$ from a material A to B is given by:

$$F_{A \rightarrow B}(T) = \int f_{BE}(\omega, T) \hbar \omega \tilde{N}_{A \rightarrow B}(\omega) d\omega \quad (3)$$

Where $f_{BE}(\omega, T)$ is the Bose-Einstein phonon distribution at an angular frequency ω and a temperature T . $\tilde{N}_{A(B) \rightarrow B(A)}(\omega)$ is an interface-dependent parameter that has the unit of a spectral particle flux, expressed as:

$$\tilde{N}_{A \rightarrow B}(\omega) = \frac{1}{2} \sum_{m=1}^{N_A} \iiint_{BZ_A} T_{A \rightarrow B}(\vec{q}_{\parallel}, \omega, m) \delta(\omega(\vec{q}_i, m) - \omega) |\vec{v}_g(\vec{q}_i, m) \cdot \vec{n}| \frac{d\vec{q}_i}{(2\pi)^3} \quad (4)$$

Where \vec{q}_i is a wave vector belonging to the first Brillouin Zone (BZ) of material A, m the mode index, N_A the number of modes in material A, δ the Dirac distribution, $\vec{v}_g(\vec{q}_i, m)$ the group velocity and \vec{n} a unit vector perpendicular to the interface.

The interfacial thermal conductance $G(T)$ is deduced from Eq. 3, which gives:

$$G(T) = \int \frac{\partial f_{BE}(\omega, T)}{\partial T} \hbar \omega \tilde{N}_{A \rightarrow B}(\omega) d\omega \quad (5)$$

According to Eqs. 3 and 5, it can be noticed that the temperature-dependence of thermal flux and conductance comes only from the occupation function f_{BE} . Thus, from the knowledge of the material-dependent parameter $\tilde{N}_{A \rightarrow B}(\omega)$, a supplementary one-

dimensional integration (over the angular frequency ω) allows us to compute both thermal flux and interfacial conductance for any temperature.

II.2. Full-Band Pseudo AMM

In AMM, the phonon mode must be conserved and thus the transmission coefficient is mode-dependent. However, this conservation is strictly possible only when the two materials on each side of the interface have the same crystallographic phase, e.g. for the monotype interface Si-3C/Ge-3C. Otherwise, finding the similarity of the phonon modes between both materials having different crystallographic structures is complex, especially when they do not have the same number of modes as it is the case in the polytype interface Ge-3C/Ge-2H.

Thus, we propose to relax the strict application of the AMM principles and let the phonons be able to change their mode when they cross the interface. This mode change can be attributed to the occurrence of some scattering mechanisms located at the interface. We have called this approach Pseudo-AMM (PAMM).

In PAMM, the definition of the relevant number of modes $N_{i(r/t),j}^{PAMM}$ present in Eq. 1 is different from that in AMM. It corresponds to the summation over all the waves with the same ω and $\vec{q}_{//}$ whatever their mode, i.e. $N_{i(r/t)}^{PAMM} = \sum_m N_{i(r/t)}^{AMM}$. By applying these modifications, the PAMM transmission expression is similar to Eq. 2 but without the mode-dependence, and the PAMM thermal flux is the same as in Eq. 3 but without the summation over the modes m . As the degree of freedom in transmission is higher in PAMM than in AMM, this leads to a higher interface conductance as it will be shown in the result section.

II.3. Full-Band DMM

In contrast to AMM postulates, within Diffusive Mismatch Model the interface is assumed to exhibit many defects able to scatter phonons and completely break their wave coherence. Thus, the phonon transmission is systematically assumed to result from a diffusive process on, i.e. each phonon reaching the interface undergoes a randomizing scattering mechanism. In other words, the wave vector and the mode of the transmitted or reflected phonon are fully independent of the incident phonon that collides the interface: there is no memory effect. The phonon energy is the only quantity to be conserved. These assumptions make the transmission coefficient only dependent on the incident phonon energy. Reddy and co-workers [25] were the first authors to adapt the DMM to a Full-Band dispersion and the only ones to use it, as far as we know.

Assuming that the transmission coefficient $T_{A \rightarrow B}(\omega)$ in Eq. (4) only depends on angular frequency ω , within the formalism of Eq. (3), the particle flux takes the simple form:

$$\tilde{N}_{A \rightarrow B}(\omega) = I_{A, \vec{n}}(\omega) \times T_{A \rightarrow B}(\omega) \quad (6)$$

with

$$I_{A, \vec{n}}(\omega) = \frac{1}{2} \sum_{m=1}^{N_A} \iiint_{BZ_A} \delta(\omega(\vec{q}_i, m) - \omega) |\vec{v}(\vec{q}_i, m) \cdot \vec{n}| \frac{d\vec{q}_i}{(2\pi)^3} \quad (7)$$

It can be noticed that we have introduced a material-dependent parameter $I_{A, \vec{n}}(\omega)$ that is referred as the DMM impedance. $I_{A, \vec{n}}(\omega)$ includes all the relevant information about the FB dispersion at a given angular frequency ω , considering a direction perpendicular to the interface \vec{n} .

Combining the principle of detailed balance, i.e. $\tilde{N}_{A \rightarrow B}(\omega) = \tilde{N}_{B \rightarrow A}(\omega)$, and the relation $T_{A \rightarrow B}(\omega) + T_{B \rightarrow A}(\omega) = 1$ that is another assumption underlying the classic DMM leads to the expression of the FB-DMM transmission as:

$$T_{A \rightarrow B}(\omega) = \frac{I_{B, \vec{n}}(\omega)}{I_{A, \vec{n}}(\omega) + I_{B, \vec{n}}(\omega)} \quad (8)$$

This yields

$$\tilde{N}_{A \rightarrow B}(\omega) = \tilde{N}_{B \rightarrow A}(\omega) = \frac{I_{A, \vec{n}}(\omega) \times I_{B, \vec{n}}(\omega)}{I_{A, \vec{n}}(\omega) + I_{B, \vec{n}}(\omega)} \quad (9)$$

It should be noted that increasing the DMM impedance of only one of the materials involved in the interface leads to higher particle flux, higher thermal flux (from Eq. 3) and thus higher interfacial conductance (from Eq. 5).

The spectral Full Band DMM impedances are plotted in FIG. 2 for the cubic (3C) and hexagonal (2H) phases of Ge along the most common directions of interface. These FB impedances (computed by using the ABCM) are compared to those given by an isotropic model using a Quadratic Isotropic Fit (QIF) of the FB dispersion along the [100] direction presented in Ref. [22].

Each peak corresponds to a flat phonon branch near the edge of BZ. In the QIF model, only three impedance peaks are present: the first one corresponds to the Transverse Acoustic modes (TA), the second to a mixing between the Longitudinal Acoustic modes (LA) and the Longitudinal Optical modes (LO) and the third one to the Transverse Optical modes (TO). Within the Full Band model, the LA and LO peaks are only degenerate near the X point. Besides, the main LA peak is several THz higher in QIF than in FB. The TA and TO peaks are higher and thinner in QIF than in FB due to the degeneracy of the transverse modes only along the [100] direction.

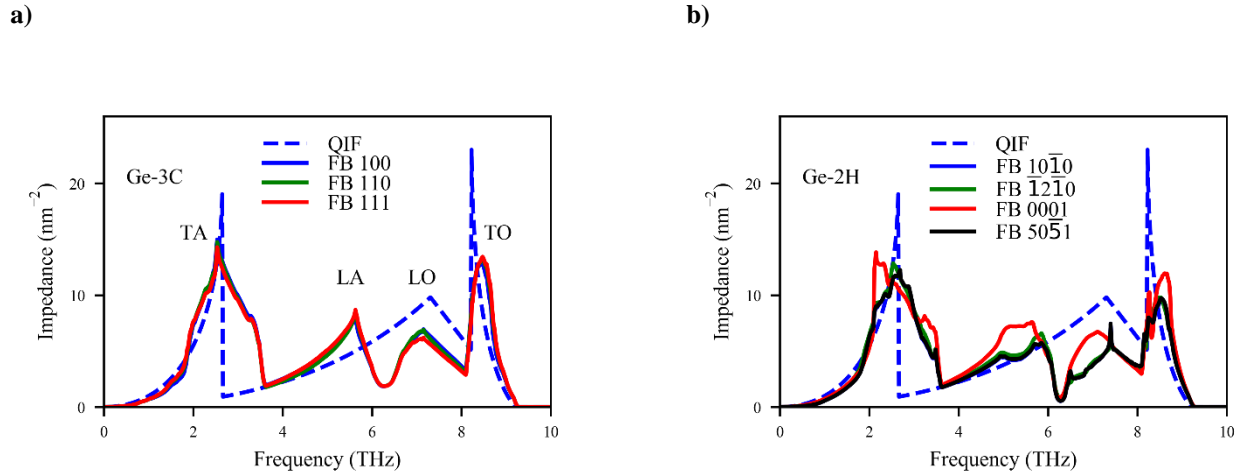


FIG. 2: FB-DMM spectral impedances for several interface orientations. Ge in a) Phase 3C and b) Phase 2H. The dashed blue lines stand for the simple Quadratic Isotropic Fitting (QIF).

Within the FB models, the impedance of the 3C and 2 H phases of Germanium have almost the same spectral distribution. Even if there are twice more modes in 2H-Ge than in 3C-Ge, their contributions are superimposed and four main peaks finally arise. They are close to those observed in the case of 3C-Ge, both in terms of frequency and intensity. Those peaks correspond to spectral windows in which the heat can efficiently transfer through the heterojunction. A good transmission between two materials is achieved when the materials have their DMM impedance peaks around the same frequencies. Besides, it can be observed that the FB impedance in the 3C phase does not depend on the interface orientation. Differently, the 2H-Ge impedance depends more significantly on the orientation and [0001] impedance is the highest.

III. SI AND GE INTERFACE & ORIENTATIONS

In this part, interfaces between silicon-3C and germanium-3C are studied. As all materials forming the interface have the same 3C structures, the number of phonon modes is equal to 6 on each side of the interface. Thus, the phonon polarizations are also identical and the conservation of mode required by the AMM can be strictly applied. Several crystalline orientations along

[100], [110] and [111] were investigated by comparing the results from FB-AMM, PAMM and DMM with previously published experimental data.

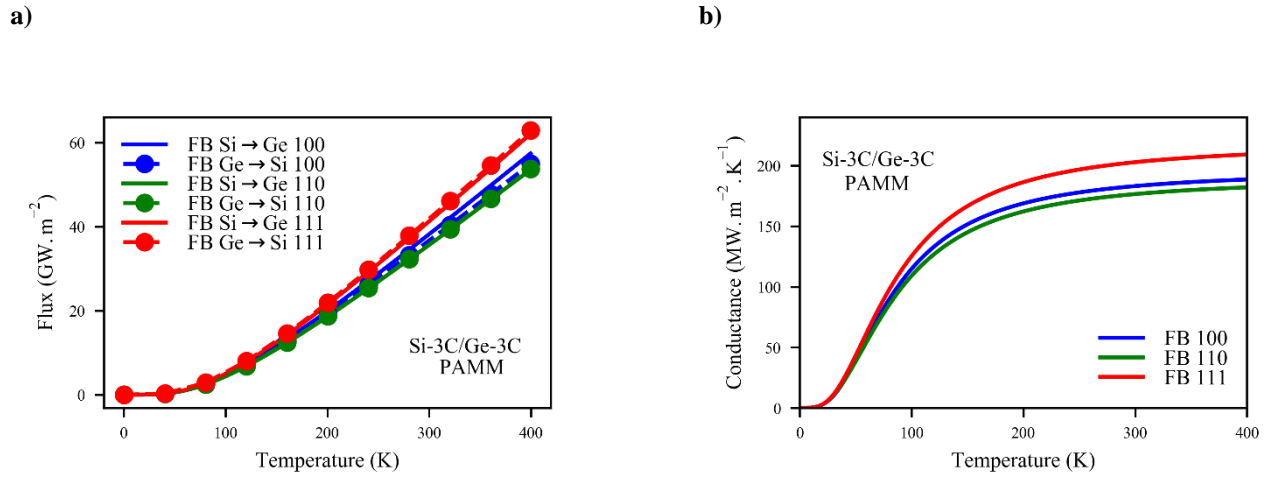
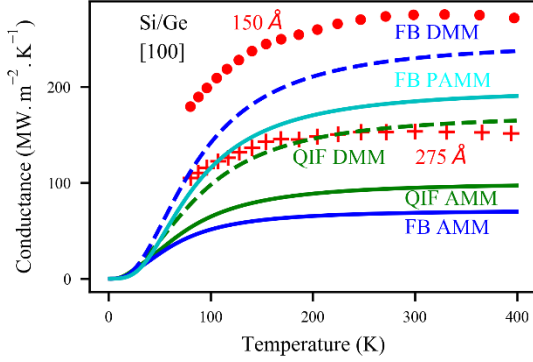


FIG. 3: a) Thermal flux and b) conductance FB-PAMM (limited to the first Brillouin Zone) at a Si/Ge interface for several orientations.

The thermal flux from Si to Ge (Si \rightarrow Ge) and from Ge to Si (Ge \rightarrow Si) computed using PAMM is plotted in FIG. 3.a for different crystalline orientations. The thermal flux passing through the interface in both directions (Si \rightarrow Ge and Ge \rightarrow Si) are equal. Thus, even if PAMM does not meet the principle of detailed balance for each frequency (as the DMM does) by construction, the total thermal flux, given by the difference between the opposite thermal fluxes, is zero at equilibrium when no temperature bias is applied.

The interfacial thermal conductance obtained from PAMM for different orientations is plotted in FIG. 3.b. Consistently with this approach, a dependence on the crystal orientation is observed in the full range of temperature because the interface breaks the central symmetry of the crystal. This dependence is not captured by DMM (not shown) as the transmission just depends on the angular frequency of the incident wave vector. The highest interfacial thermal conductance, together with the highest unidirectional thermal flux as shown in FIG. 3.a, is obtained along the direction [111] while the smallest one is along [110].

a)



b)

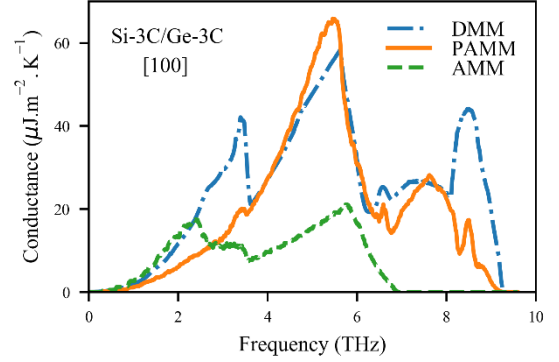


FIG. 4: a) Kaptiza Thermal conductance of the Si/Ge interface as a function of temperature for different models. Lines this work, red symbols measurements for [100] from [26] for different superlattice periods and b) different computed spectral conductances at a Si/Ge interface along a plan [100].

The values of interfacial thermal conductance obtained by using AMM, PAMM and DMM with both FB dispersions and quadratic isotropic fitting (QIF) along the [100] direction are plotted in FIG. 4.a and compared with experimental data reported by Lee et al. [26]. In this work, experimental thermal conductivities of Si-3C/Ge-3C superlattices stacked along the direction [100] are effective conductivities resulting from mixing the contributions of material and interfacial conductances. If the period of the superlattice is long enough, the effects of phonon wave coherence (confinement, interference...) are negligible. Under this assumption of fully incoherent transport, the resulting interfacial conductance can be directly compared to our calculation for a single-interface structure. Accordingly, to extract the Si/Ge interfacial conductance $G_{Kapitza}$ from the total conductivity κ_{Global} measured in Ref. [26] for relatively long period lengths of 150 and 275 Å, we have considered four thermal conductances in series in each period of the superlattice. The series is made of two interfacial conductances for the two Si/Ge interfaces plus the two layer conductances for Si and Ge layers. The interfacial thermal conductance $G_{Kapitza}$ is then given by:

$$G_{Kapitza} = 2 \left(\frac{L_p}{\kappa_{Global}} - \frac{L_{Si}}{\kappa_{Si}} - \frac{L_{Ge}}{\kappa_{Ge}} \right)^{-1} \quad (10)$$

Where L_{Si} is the thickness of silicon layer, L_{Ge} and the thickness of germanium layer, $L_p = L_{Si} + L_{Ge}$ is the period length, κ_{Si} the thermal conductivity of bulk 3C-silicon and κ_{Ge} the thermal conductivity of bulk 3C-germanium both reported in Ref. [27]. It is observed in FIG. 4a that all our models give values in the order of magnitude of those extracted from experiments. Besides, theoretical values are lower than experimental data with a short period of 15 nm for which coherent effects (phonon interference...) are probably persistent and beneficial to the thermal conductance. Moreover, all models and experiments

provide similar evolutions of the interfacial conductance and two different regimes can be identified. At low temperature, the conductance strongly increases when the temperature increases and at high temperature, higher than the Debye temperature, all the thermal conductivities tend to saturate which means that all possible phonon transmission channels are activated. It should be noticed that the presented models are unable by construction to investigate the very high temperature regime above 400-500 K where the interface scattering mechanisms become temperature-dependent, as reported for instance in [16].

In the case of a Si/Ge interface, FB-AMM and FB-DMM provide interfacial conductances that are significantly different: 60 and 220 MW/m²/K, respectively. The FB-PAMM, that is based on a mixing between AMM and DMM postulates, which does not imply a strict conservation of the wave coherence, gives intermediate results between PAMM and DMM that are closer to experimental data for a superlattice with a 27.5 nm-long period. Simple AMM and DMM calculations using Quadratic Isotropic Fitting (QIF) of the dispersion along [100], averaging the material properties, give results closer to experimental data. Nevertheless, this isotropic model is not relevant to investigate the effect of the crystal orientations and the apparent better agreement with experimental data may be considered as incidental. Full-band PAMM reasonably provides results in between that of purely coherent (AMM) and purely diffusive (DMM) transport models, in satisfying agreement with experimental results. Additionally, it is able to include anisotropic effects.

The spectral conductances, allowing us to identify the main phonon modes involved in heat transfer across the interface, are plotted in FIG. 4.b for FB-AMM, FB-PAMM and FB-DMM. In all models, the 5.5 THz channel is the dominant one and results from the LA peak in the density of states (DOS) of Ge and the TA peak in the DOS of Si [20]. This channel is especially effective in the case of PAMM spectral conductance. However, in DMM spectral conductance, secondary channels around 3 and 9 THz, corresponding to the TA peak of the Ge DOS and the LO peak of the Ge DOS, respectively, are strong too, which explains the high total conductance obtained using this model. According to standard AMM postulates, the frequency range of transmission is limited by the lowest maximum frequency of modes in one of the two materials, i.e. below 7 THz for Ge in this case. Moreover, even in the allowed energy bands, the AMM transmission and spectral conductance are lower than with the other models.

As the spectral distribution of the phonon conductance at an interface depends on the model used (AMM, PAMM or DMM), its shape could be interpreted as related to the quality of the interface. Thus, an interface exhibiting a distribution close to that of AMM is associated with a quasi-ideal interface while a distribution close to that of DMM reveals the presence of many

defects. For instance, the importance of the 5.5 THz peaks can be used as an indirect parameter to evaluate the quality of an interface.

IV. POLYTYPE GE INTERFACE & ORIENTATIONS

In this kind of interface, the mismatch of phonon modes between the two sides is not due to a change in atomic mass but just to a change of crystallographic structure. As in such polytype structure, the strict conservation of phonon mode underlying AMM cannot be applied, polytype interfaces Ge-3C/Ge-2H with different orientations are investigated here by using both DMM and PAMM.

The thermal conductances of Ge polytype interfaces are plotted in FIG. 5.a (PAMM) and FIG. 5.b (DMM) as a function of the temperature for different crystalline interface orientations. The interface [111]/[0001] is a simple “ABCABC/ABAB” stack that could be quite easily implemented in atomistic simulation such as Ab-Initio or Molecular Dynamic simulation, thanks to the limited size of the unit cell. Other three interfaces orientation are more complex and their atomistic simulation would require a much bigger unit cell. However, these orientations correspond to those experimentally observed in Ref. [13].

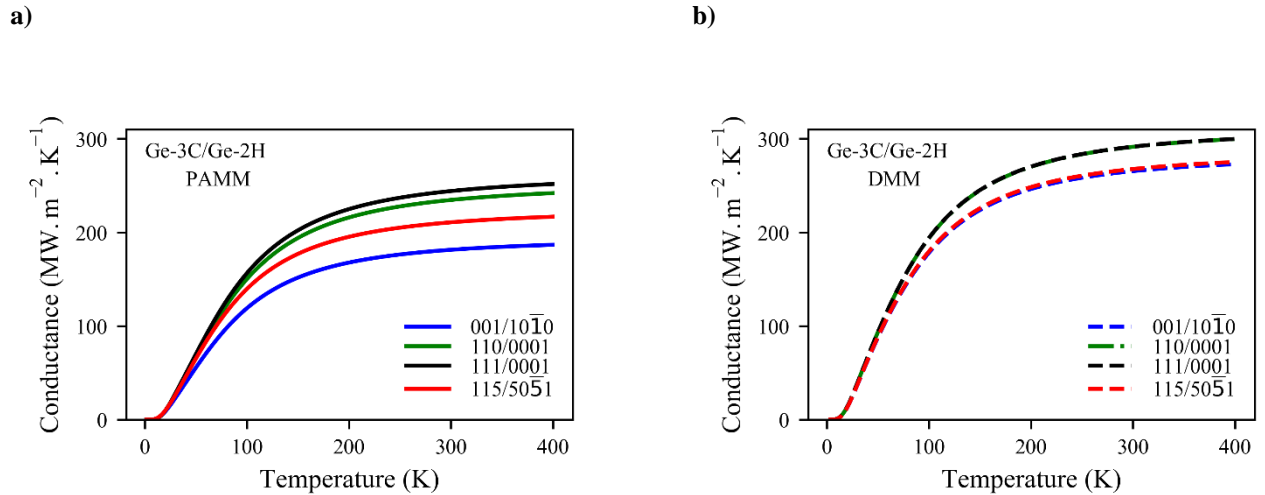


FIG. 5: Interfacial thermal conductance at the polytype Ge interface as a function of temperature for different interface orientations with the FB dispersions. Computed within a) PAMM and b) DMM.

FB-PAMM and FB-DMM estimations of the interfacial conductance are relatively close reinforcing the credibility of our estimations. Besides, the orientation of the interface has an impact on the thermal conductance. Although this orientation effect is stronger within PAMM, as the 2H phase has much less symmetry than the 3C, it is however present in DMM. The lowest conductance is obtained in the cases of $[115]_{3C}$ and $[001]_{3C}$, that are the experimental interfaces mainly observed in Ref. [13].

The most striking result is that the order of magnitude of the polytype interface conductance is similar to that of Si/Ge interface, i.e. in the order of 250 MW/m²/K. Hence, such polytype interfaces should be a promising option to reduce the thermal conductance, in particular in systems with many interfaces as the nanowires shown in Ref.[13], with a good potential for thermoelectric applications.

V. CONCLUSION

In this work, the heat transfer across Si/Ge and Ge polytype interfaces along several orientations has been investigated by using a phonon dispersion calculated in the Full 3D Brillouin Zone. To compute the phonon transmission and the related interfacial thermal conductance, Full Band extensions of the Acoustic Mismatch Model and the Diffusive Mismatch Model were used. As a complement to the FB-DMM previously derived by Reddy et al. [25], the derivation of FB-AMM and of a FB-Pseudo-AMM more relevant for considering polytype interfaces of single material have been presented here. The Full Band dispersions of bulk materials were computed using the atomistic ABCM approach for Si and Ge in both cubic (3C) and hexagonal (2H) phases.

In the case of monotype Si/Ge interface, the results obtained from the different models were compared to experimental data. AMM, that assumes a perfect interface, leads to conductance value significantly lower than available experimental data. Differently, FB-DMM and FB-PAMM results are in the range of experimental uncertainty and they are shown to be more relevant than simple isotropic models to investigate heat transport across realistic interfaces.

In the case of polytype Ge-3C/Ge-2H systems, according to our calculations, the influence of interface orientation on the thermal conductance is significant. It is shown that the orientations corresponding to experimental polytype configurations exhibit the lowest conductance. More importantly, in all studied cases, the value of the conductance in polytype interface remains in the same order of magnitude as that of the Si/Ge interface. Thus, an interface with a structural mismatch is able to limit heat transfer as efficiently as an interface with a mass mismatch. This property is very promising with a view to nanoscale thermoelectric applications.

ACKNOWLEDGMENTS

This work is supported by a public grant overseen by the French National Research Agency (ANR) through project NOE (12JS03-006-01) and as part of the “Investissements d’Avenir” program (Labex NanoSaclay, reference: ANR-10-LABX-0035).

REFERENCES

- [1] “Annual Review of Heat Transfer,” vol. 17, Begell House, 2014.
- [2] F. Bonetto, J. L. Lebowitz, L. Rey-Bellet, and others, “Fourier’s law: a challenge to theorists,” *Math. Phys.*, vol. 2000, pp. 128–150, 2000.
- [3] T. Thu Trang Nghiêm, J. Saint-Martin, and P. Dollfus, “New insights into self-heating in double-gate transistors by solving Boltzmann transport equations,” *J. Appl. Phys.*, vol. 116, no. 7, p. 074514, Aug. 2014.
- [4] P. Kapitza, “The study of heat transfer in helium II,” *J PhysUSSR*, vol. 4, no. 1–6, pp. 181–210, 1941.
- [5] E. T. Swartz and R. O. Pohl, “Thermal boundary resistance,” *Rev. Mod. Phys.*, vol. 61, no. 3, p. 605, 1989.
- [6] K. Yamane, T. Kobayashi, Y. Furukawa, H. Okada, H. Yonezu, and A. Wakahara, “Growth of pit-free GaP on Si by suppression of a surface reaction at an initial growth stage,” *J. Cryst. Growth*, vol. 311, no. 3, pp. 794–797, Jan. 2009.
- [7] A. Talneau *et al.*, “Atomic-plane-thick reconstruction across the interface during heteroepitaxial bonding of InP-clad quantum wells on silicon,” *Appl. Phys. Lett.*, vol. 102, no. 21, p. 212101, May 2013.
- [8] G. Roelkens *et al.*, “III-V/Si photonics by die-to-wafer bonding,” *Mater. Today*, vol. 10, no. 7, pp. 36–43, 2007.
- [9] P. Pichanusakorn and P. Bandaru, “Nanostructured thermoelectrics,” *Mater. Sci. Eng. R Rep.*, vol. 67, no. 2–4, pp. 19–63, 2010.
- [10] A. N. Hanna, H. M. Fahad, and M. M. Hussain, “InAs/Si hetero-junction nanotube tunnel transistors,” *Scientific reports*, vol. 5, p. 9843, 2015.
- [11] S. S. Iyer, *et al.* Heterojunction bipolar transistors using Si-Ge alloys. *IEEE Transactions on Electron Devices*, 1989, vol. 36, no. 10, p. 2043-2064.
- [12] F. J. Lopez, U. Givan, J. G. Connell, and L. J. Lauhon, “Silicon Nanowire Polytypes: Identification by Raman Spectroscopy, Generation Mechanism, and Misfit Strain in Homostructures,” *ACS Nano*, vol. 5, no. 11, pp. 8958–8966, Nov. 2011.
- [13] L. Vincent *et al.*, “Novel Heterostructured Ge Nanowires Based on Polytype Transformation,” *Nano Lett.*, vol. 14, no. 8, pp. 4828–4836, Aug. 2014.
- [14] A. Alkurdi, S. Pailhès, and S. Merabia, “Critical angle for interfacial phonon scattering: Results from *ab initio* lattice dynamics calculations,” *Appl. Phys. Lett.*, vol. 111, no. 9, p. 093101, Aug. 2017.
- [15] S. Merabia and K. Termentzidis, “Thermal conductance at the interface between crystals using equilibrium and nonequilibrium molecular dynamics,” *Phys. Rev. B*, vol. 86, no. 9, Sep. 2012.
- [16] E. S. Landry and A. J. H. McGaughey, “Thermal boundary resistance predictions from molecular dynamics simulations and theoretical calculations,” *Phys. Rev. B*, vol. 80, no. 16, Oct. 2009.
- [17] Y. Chalopin, K. Esfarjani, A. Henry, S. Volz, and G. Chen, “Thermal interface conductance in Si/Ge superlattices by equilibrium molecular dynamics,” *Phys. Rev. B*, vol. 85, no. 19, May 2012.
- [18] Yue, Y., Zhang, J., Xie, Y., Chen, W., Wang, X., “Energy coupling across low-dimensional contact interfaces at the atomic scale”. *Int. J. Heat Mass Transf.*, vol. 110, pp. 827–844, 2017.
- [19] W. A. Little, “The transport of heat between dissimilar solids at low temperatures,” *Can. J. Phys.*, vol. 37, no. 3, pp. 334–349, 1959.
- [20] D. Singh, J. Y. Murthy, and T. S. Fisher, “Effect of phonon dispersion on thermal conduction across Si/Ge interfaces,” *J. Heat Transf.*, vol. 133, no. 12, p. 122401, 2011.
- [21] W. Weber, “Adiabatic bond charge model for the phonons in diamond, Si, Ge, and α -Sn,” *Phys. Rev. B*, vol. 15, no. 10, p. 4789, 1977.
- [22] J. Larroque, B. Davier, P. Dollfus and J. Saint-Martin, “Full-Band modelling of phonons in polytype Ge and Si” ,” *EDISON 20, Buffalo, N.Y. USA, July 16-21 2017, J. Phys.: Conf. Ser. 906 012007*.
- [23] L. Lindsay and D. A. Broido, “Three-phonon phase space and lattice thermal conductivity in semiconductors,” *J. Phys. Condens. Matter*, vol. 20, no. 16, p. 165209, Apr. 2008.
- [24] A. Valentin, J. Sée, S. Galdin-Retailleau, and P. Dollfus, “Study of phonon modes in silicon nanocrystals using the adiabatic bond charge model,” *J. Phys. Condens. Matter*, vol. 20, no. 14, p. 145213, Apr. 2008.
- [25] P. Reddy, K. Castelino, and A. Majumdar, “Diffuse mismatch model of thermal boundary conductance using exact phonon dispersion,” *Appl. Phys. Lett.*, vol. 87, no. 21, p. 211908, 2005.
- [26] S.-M. Lee, D. G. Cahill, and R. Venkatasubramanian, “Thermal conductivity of Si–Ge superlattices,” *Appl. Phys. Lett.*, vol. 70, no. 22, p. 2957, 1997.
- [27] C. J. Glassbrenner and G. A. Slack, “Thermal conductivity of silicon and germanium from 3 K to the melting point,” *Phys. Rev.*, vol. 134, no. 4A, p. A1058, 1964.